Mössbauer Sidebands by rf Excitation of Magnetic Materials

Loren Pfeiffer
Bell Telephone Laboratories, Murray Hill, New Jersey 07974

and

Neil D. Heiman*†
Physics Department, College of William and Mary, Williamsburg, Virginia 23185
and Physics Department, Johns Hopkins University, Baltimore, Maryland 21218

and

J. C. Walker†
Physics Department, Johns Hopkins University, Baltimore, Maryland 21218

(Received 17 January 1972)

The phenomenon of frequency-modulation (FM) sidebands induced with rf fields in the Mössbauer spectra of ferromagnetic materials is considered in detail. The general expression for the Mössbauer transition probability in the presence of rf acoustic vibrations is given and is derived on a quantum basis. The experimental properties of the sideband effect are reviewed and new experimental results are given. Experiments show that FM sidebands are caused by the generation of rf acoustic vibrations in the sample. The sideband effect is shown to vanish in an $FeBO_3$ sample if it is heated above the Curie temperature or in an α-Fe_2O_3 sample if it is cooled below the Morin transition. The dependences of sideband formation on rf driving frequency, on rf skin depth, and on the application of additional magnetic fields are also discussed. Several previously proposed mechanisms for the generation of rf sidebands are now ruled out by these new experimental data. One mechanism which is supported by the new data is the magnetoacoustic coupling of the sample to the rf field by rf magnetostriction. This model which was suggested in our original paper and also by others is discussed in some detail. In the past the single important difficulty with the magnetostriction hypothesis has been that the rf acoustic vibrations that one calculated on a static basis from it did not have sufficient amplitude to account for the observed sideband intensities. We point out here that this difficulty with numerical magnitudes may be overcome by postulating that the primary rf magnetostrictive strain is induced in the sample plane rather than perpendicular to it as had previously been assumed. The rf acoustic vibrations resulting from this time-varying strain are then presumed to scatter within the sample so that some vibrational amplitudes come to have components along the γ-ray axis. Both the in-plane–rf-strain assumption and the acoustic-scattering assumption find support in the experimental data.

INTRODUCTION

We recently reported that when a metallic foil is subjected to an rf magnetic field, additional distinct lines appear in the Fe^{57} Mössbauer absorption pattern of that foil.[1–3] We interpreted these additional lines as frequency-modulation (FM) sidebands, where the frequency modulation results via the Doppler effect from acoustic vibrations produced by the magnetostrictive interaction of the foil with the rf magnetic field. In this paper we present the results of a more detailed investigation and analysis of this phenomenon. These new results have turned out to be in very good agreement with our original rf magnetostriction hypothesis.

Classical FM theory[4] shows that when an electromagnetic wave with a carrier frequency ω_0 is modulated sinusoidally at a frequency ω_m, the resulting frequency spectrum consists of the original carrier and an infinite set of sidebands. These sidebands are located at frequencies given by $\omega_0 \pm n\omega_m$, and their relative amplitudes are given by $J_n^2(m)$, where n is an integer, J_n is the nth ordinary Bessel function, and m is the modulation index.

Ruby and Bolef[5] were the first to produce FM sidebands in Mössbauer spectra. They did so by mechanically vibrating the source with a piezoelectric transducer. Several other investigations of FM sidebands in Mössbauer spectra have since been reported.[6–8] In all cases, either the source or the absorber was mechanically vibrated with an external piezoelectric transducer. In the experiments we report here, *no mechanical transducers are employed* to produce the acoustic vibrations. Instead the vibrations are generated *within* the absorber itself as a result of the interaction of the absorber material with the applied rf magnetic field. We wish to emphasize this distinction from the outset.

Perlow[9] in 1960 was the first to study the effects of rf magnetic fields on Mössbauer nuclei. Similar experiments were repeated with more detail in 1967 by Matthias.[10] In both experiments a Co^{57}

source in an iron matrix was attached rigidly to the iron-absorber foil. Either the source, the absorber, or both were subjected to an rf field, and the total number of 14.4-keV γ rays transmitted through the source-absorber sandwich were counted as function of frequency. In both cases the experiments reported a change in count rate at 26 MHz, the NMR frequency of the 14.4-keV level of Fe^{57}. They suggested that this count-rate change could be attributed to the distortions of the Mössbauer line produced by excited-state NMR transitions, an effect which had been predicted by Hack and Hammermesh[11] and others.[12]

In both experiments, however, there were certain anomalies in the results: (i) the rf field produced large changes in the count rate even at nonresonant frequencies, (ii) resonance effects were also observed at 45.5 MHz, the ground-state NMR frequency, and (iii) for the strength of the rf field used, the observed effects were much too large. These anomalies could not be satisfactorily explained at the time. Both authors considered the possibility that magnetostrictive effects in the iron might be responsible, and did additional experiments to test this hypothesis. Matthias[10] observed no sideband effect in a velocity spectrum taken with a single-line source and an iron absorber subjected to a 14.9-MHz field of about 4 G. Perlow[13] performed a similar experiment using a single-line absorber and sources of Co^{57} in Permalloy and Superpermalloy subjected to rf fields of 4.2 and 6.5 MHz. He observed a general washing out of the Mössbauer pattern. Perlow was able to fit the data with either of two possible mechanisms: (i) magnetostrictive sidebands or (ii) random flipping of the hyperfine field due to domain-wall passage; however, he ruled out the first mechanism because the fit required too large a value of the magnetostrictive constant.

The work reported in this paper suggests that all of the above effects observed by Perlow and Matthias are understandable in terms of the formation of magnetostrictive sidebands by the rf field. This matter was discussed in our earlier paper,[1] and will be discussed further below.

This phenomenon of magnetostrictively produced acoustic sidebands in Mössbauer spectra has also been investigated independently by Asti *et al.*[14] Their results are substantially in agreement with our interpretation.

FORMALISM OF FM DOPPLER SIDEBANDS

One can apply classical FM theory to the effect of acoustic vibrations upon Mössbauer spectra by noting that if a radiating nucleus is sinusoidally vibrated the resultant Doppler shift produces a frequency modulation of the emitted radiation. For the case of sinusoidal vibrations, the modulation index can easily be shown[5,15] to be $m = x_0/\lambda\!\!\!^{-}$, where x_0 is the maximum displacement and $\lambda\!\!\!^{-}$ is the wavelength of the γ radiation over 2π. It should be pointed out, however, that Mössbauer spectra represent an ensemble average over many nuclei. Therefore, if the amplitude of vibration x_0 is not the same for each radiating nucleus but is instead distributed over a range of values, $J_n^2(x_0/\lambda\!\!\!^{-})$ must be multiplied by the proper distribution function $P(x_0)$ and integrated over x_0. Therefore, if we define $W(E)$ to be the Mössbauer transition probability in the absence of the acoustic vibrations and $W'(E)$ as the transition probability with acoustic vibrations, we can write

$$W'(E) = \sum_{n=-\infty}^{\infty} W(E + n\hbar\omega_m) \int_0^{\infty} J_n^2\left(\frac{x_0}{\lambda\!\!\!^{-}}\right) P(x_0)\, dx_0 \,. \tag{1}$$

The averaging process has no effect upon the frequency position of the sidebands but only changes the relative amplitudes. Abragam[16] in a quantum-mechanical treatment of *incoherent* vibrations derived the following expression for $W'(E)$:

$$W'(e) = \sum_{n=-\infty}^{\infty} W(E + n\hbar\omega_m) \left[e^{-x_0^2/\lambda\!\!\!^{-2}} I_n\left(\frac{x_0^2}{\lambda\!\!\!^{-2}}\right) \right] \,, \tag{2}$$

where I_n is the Bessel function of imaginary argument. He was also able to show that Eqs. (1) and (2) are equivalent when $P(x_0)$ in Eq. (1) corresponds to a Rayleigh distribution. There have been other theoretical treatments of this subject using both classical and quantum-mechanical formalisms, most notably that of Mishory and Bolef.[8] All of these results are in complete agreement with Eq. (1). Unfortunately, Eq. (1) has come to be called the "classical" result, while Eq. (2) has been called the "quantum-mechanical" result. This nomenclature has, in our opinion, produced undue confusion in the literature on the subject by implying that Eq. (2) is more correct on theoretical grounds. To remove this confusion, we provide a completely quantum-mechanical derivation of Eq. (1) in the Appendix.

EXPERIMENTS

The apparatus used in these experiments is shown schematically in Fig. 1. The Mössbauer spectrometer is a conventional constant-acceleration type used in transmission geometry. γ rays from the Co^{57} in Pd source pass through the fixed absorber under study and are detected using a Kr-CO_2 proportional counter and conventional electronics. The rf magnetic field is applied by wrapping the absorber with about eight turns of silver wire to form a loosely wound flattened helical coil. This coil is the inductance of a tuned LC tank circuit which is fed by an amplifier-oscillator system

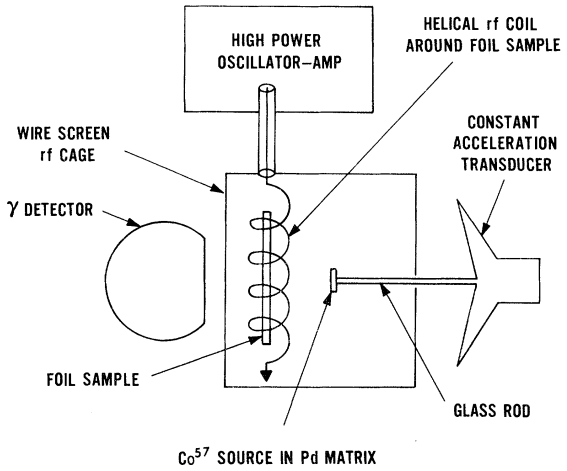

FIG. 1. Schematic diagram of experimental apparatus. The constant-acceleration transducer, Co^{57} in Pd source, absorber foil, and γ detector together form a conventional Mössbauer-effect spectrometer which is used to study the Fe^{57} nuclei in the absorber foil. A linearly polarized rf magnetic field is applied to the absorber by means of the helical wire coil and the high-power oscillator amplifier. The rf oscillator is a General Radio 1164A frequency synthesizer, and the rf amplifier is an Instruments for Industry Model No. 404A. The rf field is measured by monitoring the current through the helical coil with an rf thermocouple ammeter. The screen cage surrounding the absorber helix is necessary to prevent radiated rf power from interfering with the other electronic equipment.

capable of delivering up to 600 W of rf output.

In order to prevent radiating rf fields from interfering with the other electronics, it was necessary to enclose the source, absorber, and rf tank in a wire screen cage which was grounded to the rf coaxial shield. In most experiments it was also necessary to cool the absorber because of rf heating. Cooling was most often accomplished by directing a gentle stream of cool N_2 gas at the absorber. In the controlled-temperature experiments the absorber was immersed in a gently flowing stream of liquid freon E3 the temperature of which was maintained by a proportional controller.

The experimental data were obtained in the form of Mössbauer velocity spectra. Each of these spectra was fitted with a least-squares-fitting computer routine that contained the following assumptions and constraints: (i) All absorption lines are Lorentzian; (ii) the normal Mössbauer lines are reduced in size by the rf field; (iii) in the presence of rf perturbation each normal Mössbauer line is associated with a number of symmetric pairs of sideband satellites; (iv) the sidebands are located relative to the parent line at velocity positions corresponding to integral multiples of the applied frequency; (v) the linewidths of the sidebands are the same as the parent line; and (vi) all line intensities are free-fitting parameters subject to the constraint that all sidebands of a given order have the same intensity when expressed as an intensity ratio with the corresponding parent line. By selectively removing for a time certain of these constraints it was shown experimentally that the fitting assumptions listed above did not distort the data.

Figures 2 and 3 illustrate the basic features of the rf-sideband effect in iron metal. For Fig. 2 an rf magnetic field of 7.5-Oe peak amplitude was applied in the plane of an annealed iron-metal foil 25 μm thick by 1.25-cm diam, and the various Mössbauer spectra were obtained as a function of the driving frequency. The conditions for Fig. 3 were the same except that the iron-absorber foil in this case was 8 μm thick.

To verify that the sidebands were located relative to their parent lines by exact integral multiples of the driving frequency, the Fe^{57} hyperfine interval as determined from NMR measurements was used as a calibration test. The Fe^{57} ground-state sublevels are split by 45.49 MHz at 300 °K.[17] From this one quickly obtains that the excited-state splitting is 26.0 MHz and the splitting of the outer lines is 123.5 MHz. Using these calibration controls in the fitting program described above generated the smooth curves in Figs. 2 and 3 and showed that the sidebands are indeed displaced from their parent lines by exactly $\pm n\nu$.

One can make application of this property by using rf sidebands as a Mössbauer calibration technique. Calibration using rf sidebands has the great advantage of giving the spectroscopic energy splittings directly in frequency units, thereby circumventing all of the difficulties involved in accurately measuring the source velocity and the subsequent conversion to energy units. For ease of comparison, both velocity units and absolute-frequency units are used for most of the figures of this paper.

RESULTS

This section will contain a listing and discussion of the important experimental properties of the rf-sideband effect.

First we review the evidence which shows that rf acoustic vibrations are generated in the sample during sideband experiments. The most important single piece of evidence for acoustic vibrations is the close similarity of our magnetically induced sideband spectra with spectra in the literature[5–8] that were obtained by vibrating the entire source or absorber mechanically. This point is made in a more quantitative way by the excellent data fits of Figs. 2 and 3 which were made using the acoustic-Doppler-modulation formalism given above.

The other evidence for acoustic waves involves the dependence of the rf effect on the size of the

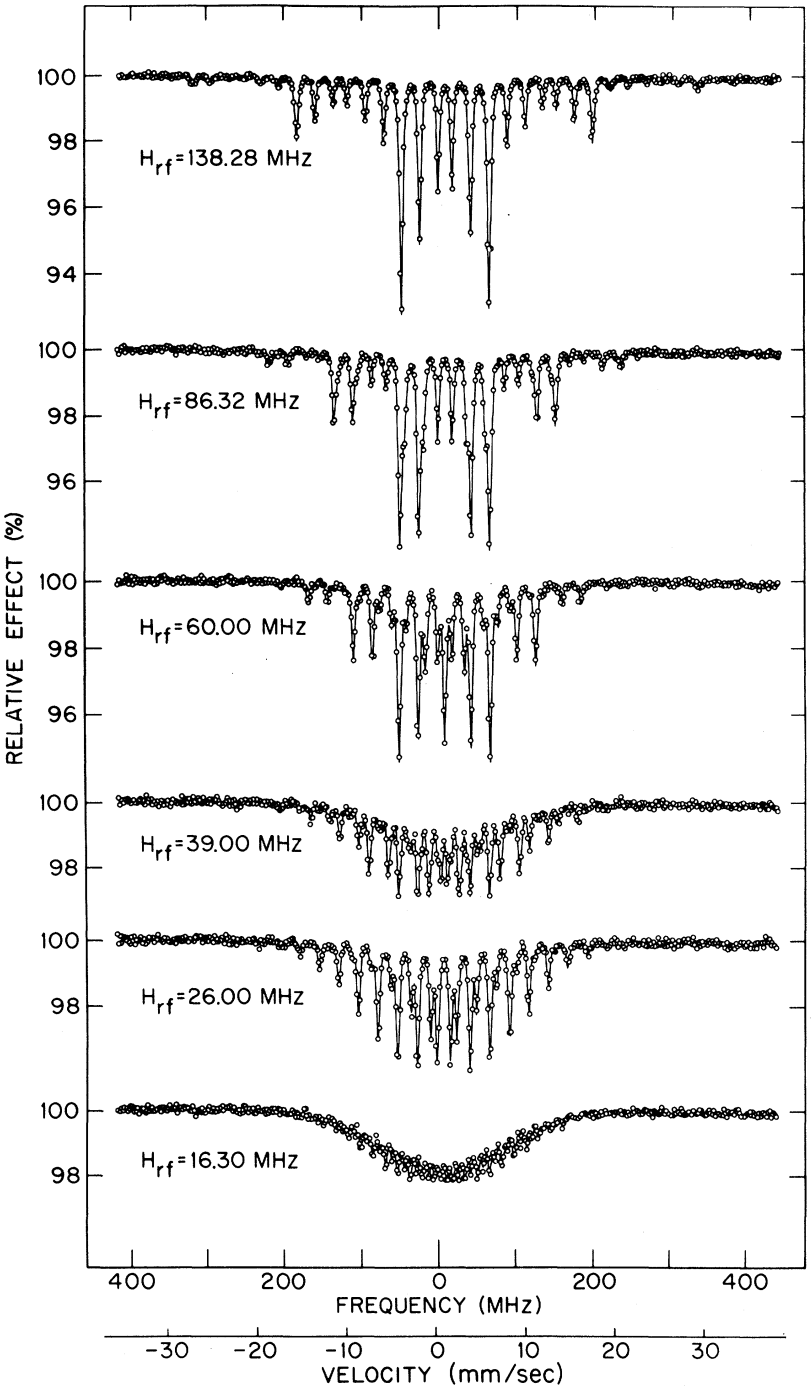

Fig. 2. rf-Mössbauer-sideband effect in a 25-μm sample foil as a function of exciting frequency. For each Mössbauer spectrum the rf magnetic field was 7.5 Oe in peak amplitude directed in the plane of the absorber. The absorber was a foil of 99.99% purity natural iron 25 μm thick and 12.5 mm in diameter, which had been previously annealed in dry hydrogen at 950 °C for several hours.

absorber particles. In the earliest work[1] it was observed that sidebands did not occur in powdered absorber materials. For example, rf sidebands are readily seen in iron-metal foils or in Fe_2O_3 single crystals, but if these materials are broken up into micron-sized particles, no rf effect is observed. This behavior is consistent with an acoustic model, since one would expect the amplitude of any internally generated acoustic vibration to be small in particles that are themselves small compared to one-half the acoustic vibration wavelength.

Of course, other physical effects such as demagnetizing fields and eddy currents are also known to depend on the size and shape of the absorber particles. To separate these effects from the acoustic particle-size effect described above, a series of special absorbers was made by slicing natural iron foils (2.0 μm thick) into mosaics of

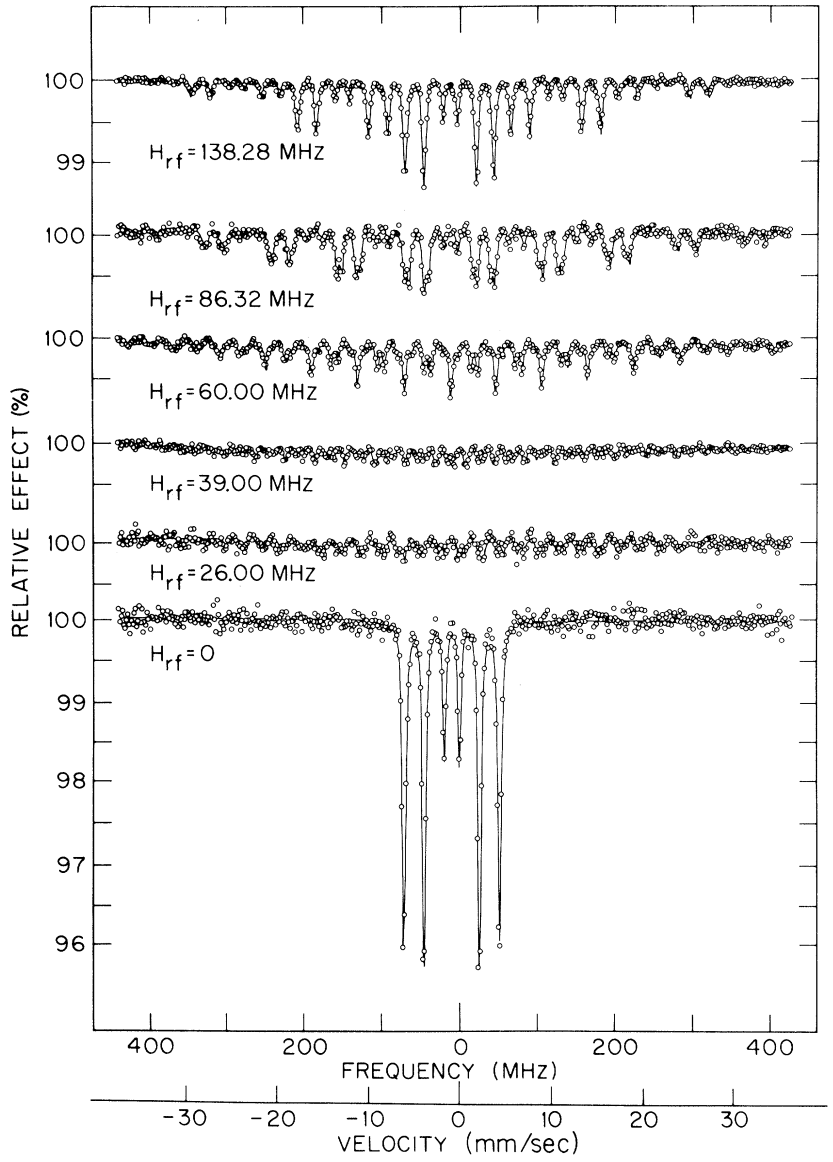

FIG. 3. rf-Mössbauer-sideband effect in an 8-μm sample foil as a function of exciting frequency. For each Mössbauer spectrum the rf magnetic field was 7.5 Oe in peak amplitude directed in the plane of the absorber. The absorber was a foil of 99.99% purity natural iron 8 μm thick and 12.5 mm in diameter, which had been previously annealed in dry hydrogen at 950 °C for several hours.

tiny squares of various sizes down to 500 μm on a side. The velocity of sound in metallic iron is $\sim 5\times10^5$ cm/sec so that 500 μm corresponds to more than five half-wavelengths of 26-MHz acoustic oscillations, but to only a quarter-wavelength of 2.5-MHz oscillations. Thus if the acoustic interpretation of the size dependence is correct, slicing the absorber foil into 500-μm squares should have little effect upon sidebands generated at 26 MHz but should significantly reduce the sideband intensity produced by a 2.5-MHz oscillating magnetic field. On the other hand, effects associated with demagnetizing fields and eddy currents are nearly independent of frequency for mosaic squares of this size and separation.

The experiments confirm the acoustic model. Slicing the foil had no apparent effect upon the sidebands produced by a 26-MHz field. It did, however, significantly reduce the sidebands produced by a 2.5-MHz field. Figure 4 shows 2.5-MHz sideband spectra as a function of the size of these mosaic squares. At 2.5 MHz the sidebands lie too close together to be cleanly resolved; nonetheless, the size dependence is clearly illustrated.

More detailed experiments of this kind were recently done using crystals of α-Fe_2O_3 which were broken into various particle sizes and sorted with sieves to obtain absorbers of uniform particle size.[18] These experiments also confirm the acoustic-vibration picture outlined above.

By way of further exploration a survey was made of the dependence of the sideband effect as each of the foil dimensions was separately varied. Foils were sliced into long strips 2 cm$\times$250 μm. For

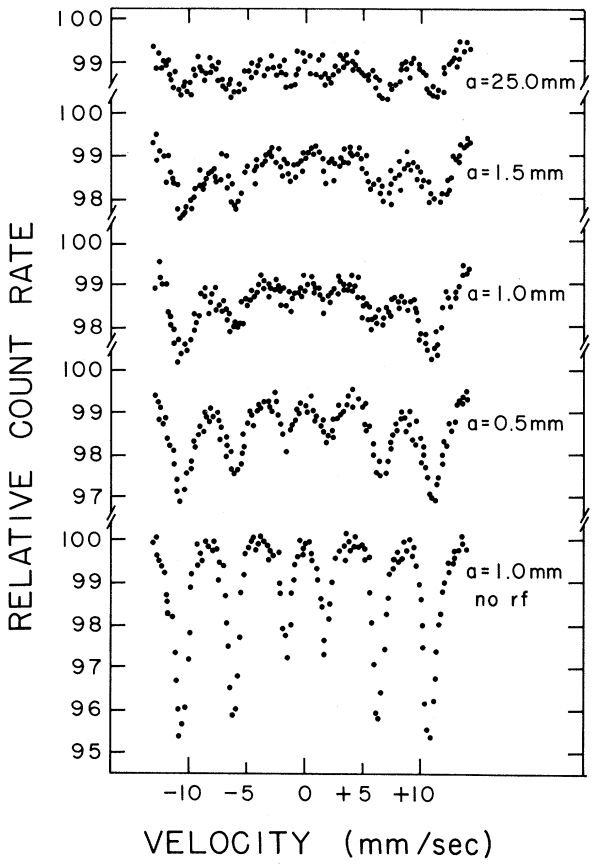

FIG. 4. Effect of foil dimensions on sideband intensity. A series of absorbers was made by mechanically slicing 2-μm-thick foils of natural iron metal into mosaics of small squares. Sideband generation was tested in each absorber at 26-MHz–12-Oe peak and also at 2.5-MHz–12-Oe peak. The 2.5-MHz rf data are shown above as a function of the length of a square in each mosaic array. The sideband-modulation indices obtained from these data are as follows: 25-mm squares, $m=1.30$; 1.5-mm squares, $m=1.20$; 1-mm squares, $m=1.10$; 0.5-mm squares, $m=0.90$. In the 25-MHz experiments no changes in the sideband effect were observed as the square sizes were discussed.

these foils the inhibition of the sideband effect at 2.5 MHz was less pronounced and was dependent upon the orientation of the strips relative to the rf magnetic vector. The smaller inhibiting effect is understandable since for the strips one of the acoustic vibrational constraints is lifted. The fact that the 2.5-MHz sidebands were nearly twice as large with the strips parallel to $\vec{H}_{rf}$ than when perpendicular is most probably due to the orientation dependence of the magnetoelastic coupling to be discussed below, but could be due to differing rf demagnetizing factors.

Sideband generation depends also on the other dimension—the foil thickness. At any given frequency as the foil thickness is increased, a larger rf field is required to produce an equivalent sideband effect. Compare the 25- and 8-μm iron-foil data in Figs. 2 and 3, for example. This is expected, because all of the loss mechanisms, demagnetizing fields, skin depth, and hysteresis increase with foil thickness. On the other hand, no sidebands could be produced in a very thin ($\lesssim 300$ Å) evaporated-iron film. This again was probably due to the lack of acoustic continuity of the film.

Additional evidence for internal acoustic vibrations is shown in Fig. 5. Here an iron foil was rotated about the rf-field vector, and the sideband intensity was observed to increase (open circles). When both the absorber and the rf field were rotated to produce a component of rf field along the γ-ray beam, the sideband effect increased more markedly (solid circles). This suggests quite reasonably that the acoustic vibrations have greater amplitudes in the plane of the foil, particularly in the direction of the rf field. It is hard to imagine some other frequency-modulation mechanism which would have this orientation dependence.

Having completed our discussion of the acoustic properties of rf sidebands, we now proceed to the magnetic properties. The sideband effect has been observed only in magnetically ordered samples. These included both metals such as iron, Permalloy, or Supermendur, and magnetic insulators such as

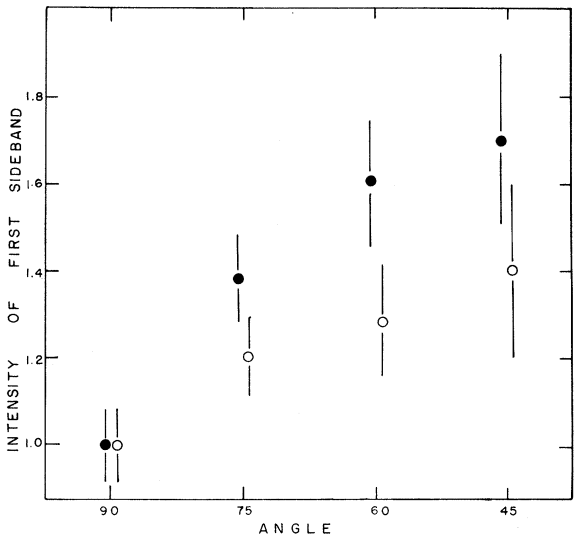

FIG. 5. Relative intensity of the first rf sideband from an iron-absorber foil as a function of the angle in degrees between the foil plane and γ rays. The open circles are obtained when the foil is rotated about the rf-field vector, which remains perpendicular to the γ-ray beam. The solid circles are obtained when both the foil and the rf-field vector are rotated about an axis perpendicular to both the rf-field vector and the γ-ray beam. This rotation produces a component of the rf field in the direction of γ-ray propagation.

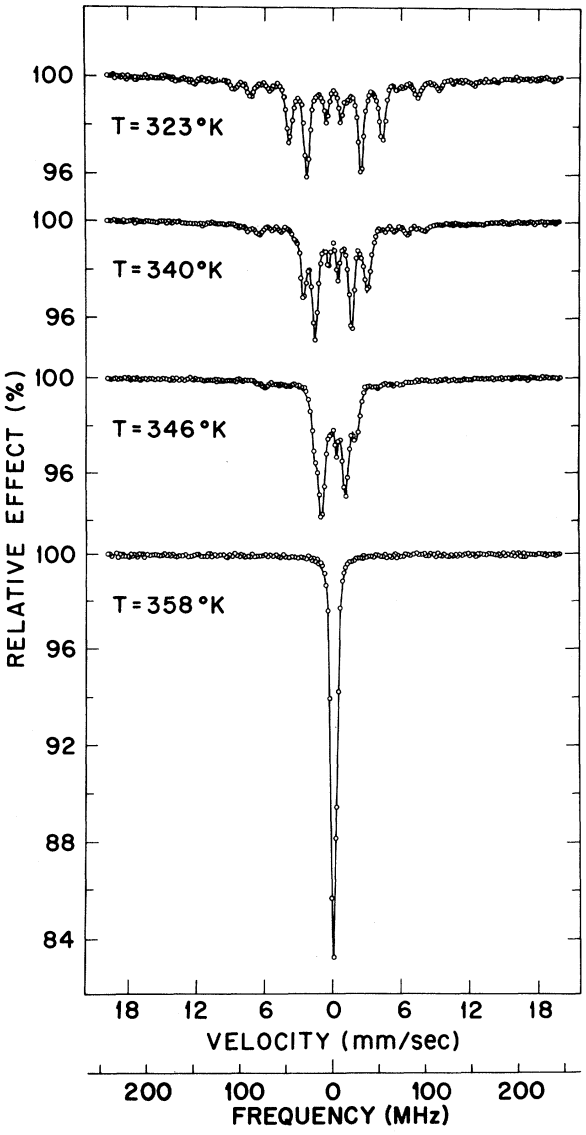

FIG. 6. Behavior of the rf-sideband effect near the Curie temperature. The rf field for all the spectra was 5.0-Oe peak amplitude at 61.0 MHz. The absorber was made from single crystals of $FeBO_3$ which (Ref. 22) has a Curie temperature of 348°K. The sample temperature was controlled using a thermocouple and a conventional resistance heater in a feedback loop as in Ref. 22.

α-Fe_2O_3, $FeBO_3$, or various ferrites.

The unimportance of sample conductivity for the sideband effect immediately rules out the class of physical mechanisms that involve eddy currents. Ruled out, for example, are effects of the type seen by Gaerttner and others[19–21] in which rf fields on metals generate acoustic waves by action of the Lorentz force on the induced currents in the skin depth.

Because the formation of rf sidebands appears to depend critically on the magnetic properties of the sample, it was decided to study this dependence in some detail by monitoring the sideband effect during various ferromagnetic phase transitions. The specific phase transitions chosen were the Curie transition in iron borate and the Morin transition in α-phase Fe_2O_3. The conclusion from these experiments is that rf sidebands are generated only if the sample has a net uncompensated ferromagnetic moment. The data are summarized in Figs. 6 and 7.

Figure 6 shows the behavior of sidebands in $FeBO_3$ single crystals subject to an applied rf magnetic field of 5.0 Oe at 61.0 MHz. In these data the applied rf field was held constant, and the sample temperature was maintained using a conventional resistance heater in a temperature feedback loop. $FeBO_3$ is a weak ferromagnet with a Curie temperature of 348 °K,[22] and indeed one sees in the figure that the sidebands disappear as the sample temperature is raised above the Curie point.

In Fig. 7 similar behavior is shown for the ferromagnetic-to-antiferromagnetic Morin transition in single crystals of Fe_2O_3. For this case as well, sidebands occur only if the sample has a net ferromagnetic moment. Above the Morin temperature the Fe_2O_3 crystals are canted ferromagnets and show the sideband effect. On the other hand, below the – 13 °C transition the crystals are antiferromagnets with no canting and the sideband effect does not occur.

Having established that the sample must be ferromagnetic, the question arises of the role of magnetic domains in sideband formation. One can most easily study this question experimentally by applying to the sample a static magnetic field $\vec{H}_0$ of sufficient amplitude to sweep away all of the domain walls leaving the sample magnetically saturated during the rf excitation.

The experiments are straightforward: One simply monitors the rf sideband effect as a function of the magnitude of the field. However, two possible systematic effects can distort the data and may have been important in earlier experiments.[2,3,14] One of these effects occurs if iron pole pieces are used in the static-field magnet. The problem is that the additional iron of the pole pieces in the vicinity of the sample changes the magnetic induction field of the rf tank coil in complicated geometry-dependent ways. This problem is particularly serious because the effect on the rf induction field depends on the degree of magnetic saturation of the pole pieces. To avoid this problem, the H_0 static field in our experiment was generated using Helmholtz coils operating without any ferromagnetic material in the flux return path.

The other precaution one must take is to determine the relationship between the amplitude of the applied field H_0 and the degree of magnetic satura-

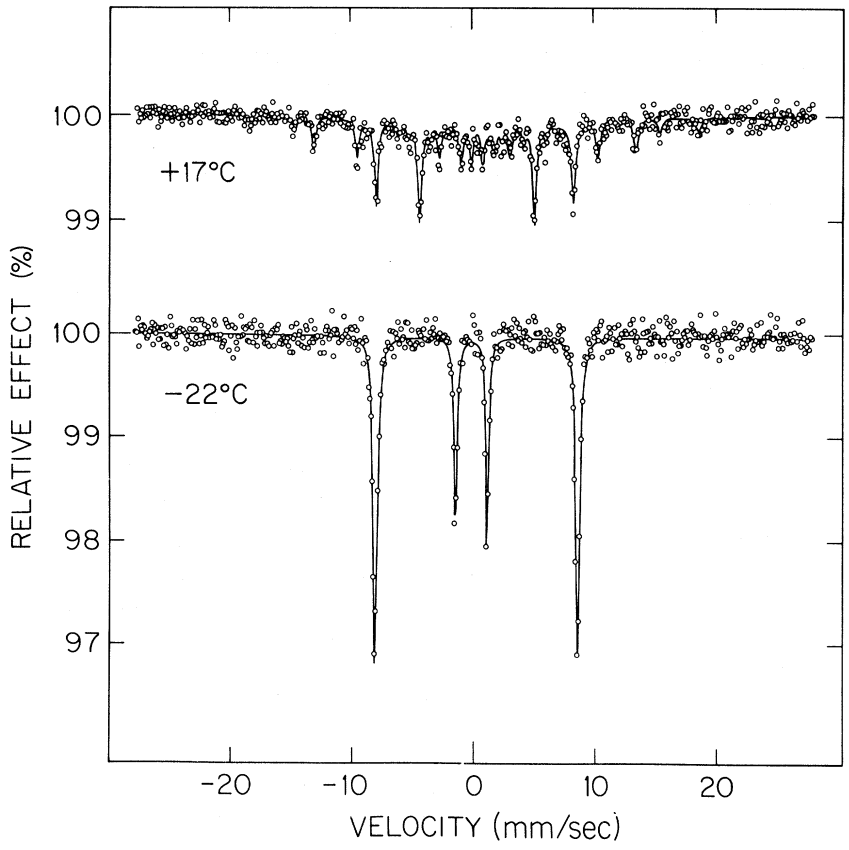

FIG. 7. Behavior of the rf-sideband effect near the Morin ferromagnetic-to-antiferromagnetic transition in single crystals of α-Fe_2O_3. The rf field for both spectra was 22-Oe peak amplitude at 61.4 MHz. The rf-sideband effect is seen at +17 °C where the Fe_2O_3 crystals are ferromagnetic, but the effect is not seen at −22 °C, where the crystals are antiferromagnetic.

tion in the absorber sample. This is important since B-H relationships, because they depend on demagnetizing and annealing effects, are functions of the specific rf sample and its history. For these reasons a separate measurement was made of the magnetic hysteresis loop of the annealed iron-foil sample used in the applied H_0 field experiments. From these data shown in Fig. 8 we see that applied H_0 fields of the order of 100 Oe are sufficient to clear our sample of nearly all internal domain walls.

With these considerations in mind, a static H_0 field was applied in the plane of the foil sample but perpendicular to the H_{rf} field. Figure 9 shows several rf-sideband Mössbauer spectra as a function of this additional H_0 field. Except for the top control spectrum, the rf field was maintained to 8-Oe peak amplitude at 85 MHz. We see that the static perpendicular field has very little effect on the formation of rf sidebands. There is a slight decrease in sideband production for $H_0 = 1000$ Oe; however, there is actually a slight increase in the rf effect for $H_0 = 320$ Oe, where as we have seen there are only a very few domains and domain walls in the sample.

This experiment, by showing that the sideband effect is independent of the number and size of domains in the sample, appears to rule out the entire class of models that invoke for sideband generation the movement of ferromagnetic domain walls. Ruled out, for example, is the domain-wall passage model[13] proposed by Perlow which was mentioned

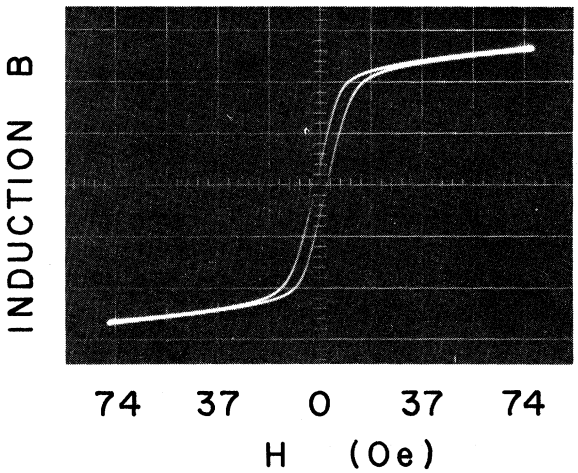

FIG. 8. $\vec{B}-\vec{H}$ hysteresis loop of the 8-μ-thick annealed iron foil used for the static-field experiments of Figs. 9 and 10. The loop shown was traced at a 60-Hz repetition rate.

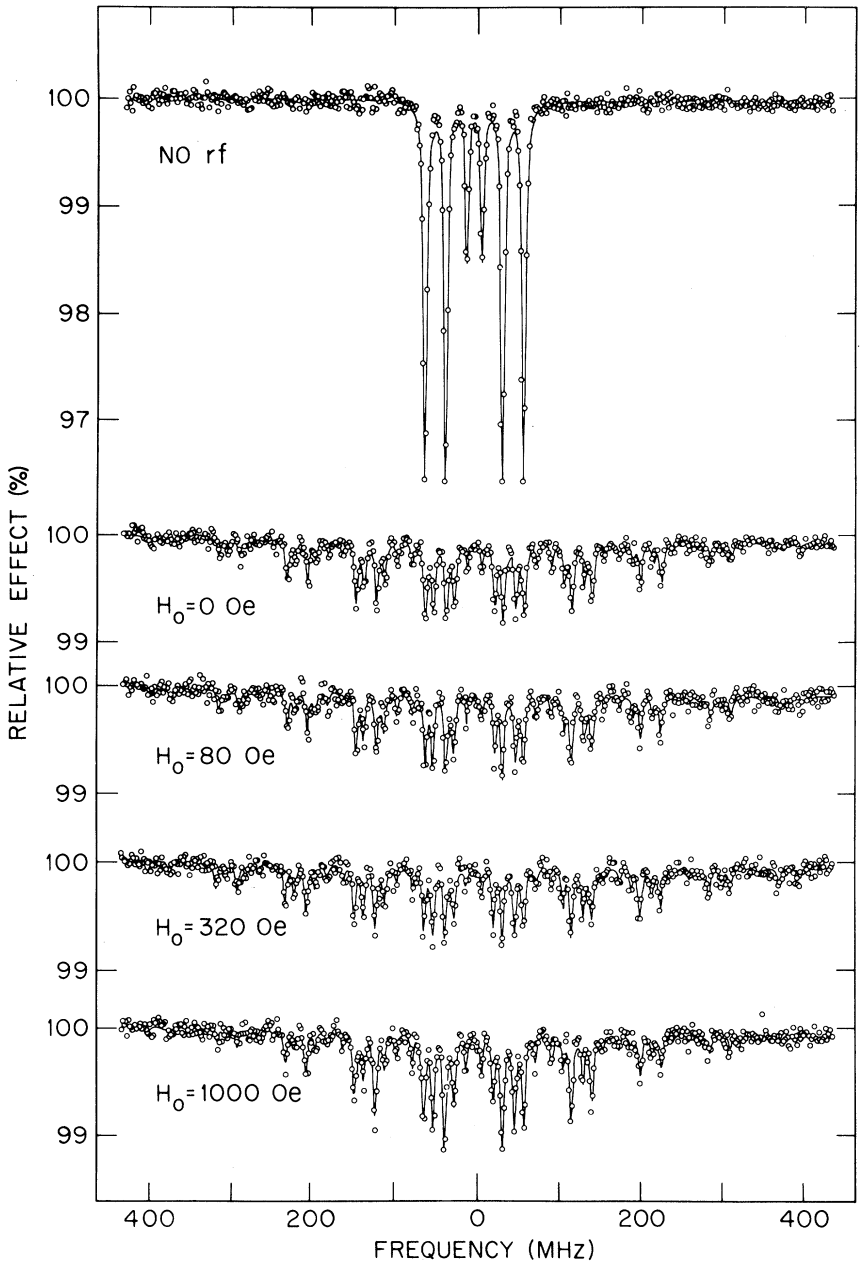

FIG. 9. Dependence of the rf-sideband effect on an additional applied field $\vec{H}_0$ oriented perpendicular to $\vec{H}_{rf}$. The rf field for each of the lower four spectra had a peak amplitude of 8 Oe at 85 MHz.

in the Introduction.

The other experiment one can do with static H_0 fields is to apply them to the sample in the direction parallel to $\vec{H}_{rf}$. Experimental spectra for this field geometry are shown in Fig. 10. These spectra show that sideband generation quenches rapidly with increasing $\vec{H}_0$ amplitude, provided $\vec{H}_0$ and $\vec{H}_{rf}$ are parallel. The reason for this behavior is discussed in the next section.

The last experimental property we discuss in this section is the dependence of rf-induced sidebands on driving frequency. A strong frequency dependence is observed, as may be seen in the data of Figs. 2 and 3 for foils of iron metal.

To display the frequency dependence quantitatively, it is useful to characterize the relative sideband effect using only a single numerical index. We know it should be possible to do this because expression (1) with the proper modulation index, x_0/π, presumably describes the sideband amplitudes of a spectrum exactly. Unfortunately, we do not know the functional form of the weighting factor $P(x_0)$. Although many trial functions have been tested, none of these generate sideband amplitudes in exact agreement with the amplitudes obtained from a least-squares computer fit to the experi-

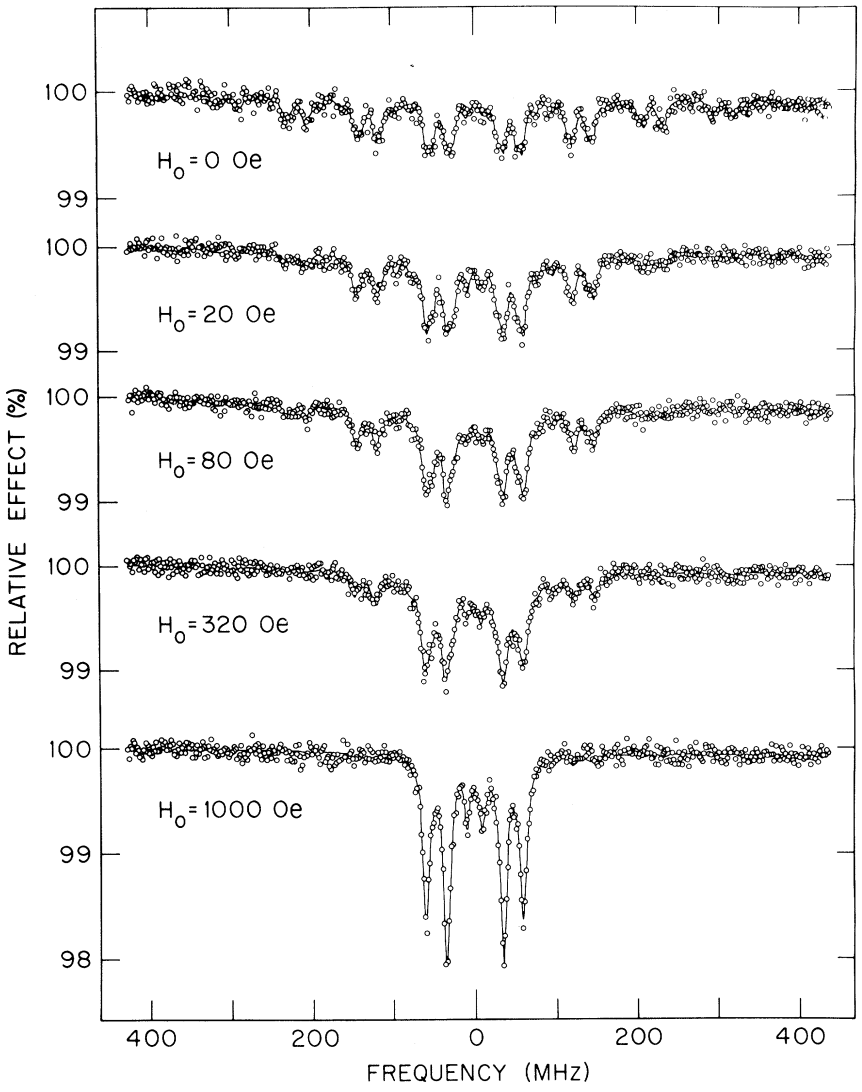

FIG. 10. Dependence of the rf-sideband effect on an additional applied field $\vec{H}_0$ oriented parallel to $\vec{H}_{rf}$. The rf field for all spectra in the figure had a peak amplitude of 8 Oe at 88 MHz.

mental data.

Some trial functions, of course, give sideband amplitudes in closer agreement with experiment than others. Thus reasonably close agreement with experiment is obtained if $P(x_0)$ is a Rayleigh distribution. In this case the resulting sideband amplitudes are given by expression (2). The agreement with experiment using a Rayleigh function is by no means exact, but it is possible using it and a single modulation index $(x_0/\pi)^2$ to generate the experimental sideband coefficients of a spectrum to within about 50%. In this way the rf-sideband effect for each spectrum is characterized at least approximately by a single numerical index.

Figure 11 is a plot of these experimentally derived modulation indices obtained from the frequency data of Figs. 2 and 3. The circle is the modulation index that gave the best fit to the zeroth-order sideband coefficient, and the vertical line extending away from it is the range of indices required to overlap all of the other orders of sideband coefficients. The length of this line then is simply a measure of how well or poorly expression (2) actually does characterize the experimental sideband coefficients.

In Fig. 11 the frequency dependence of rf sidebands in iron metal is clearly displayed. Over the rf range examined there does not appear to be any resonant behavior, but the experimental modulation indices drop monotonically by several orders of magnitude as the driving frequency is increased, varying as $1/\nu$ to the power 3 or 3.5.

The other characteristic of the data is the apparent lack of importance of the rf skin depth for the effect. The rf skin depth

$$d = \frac{1}{2\pi}\left(\frac{\rho}{\mu\nu}\right)^{1/2}$$

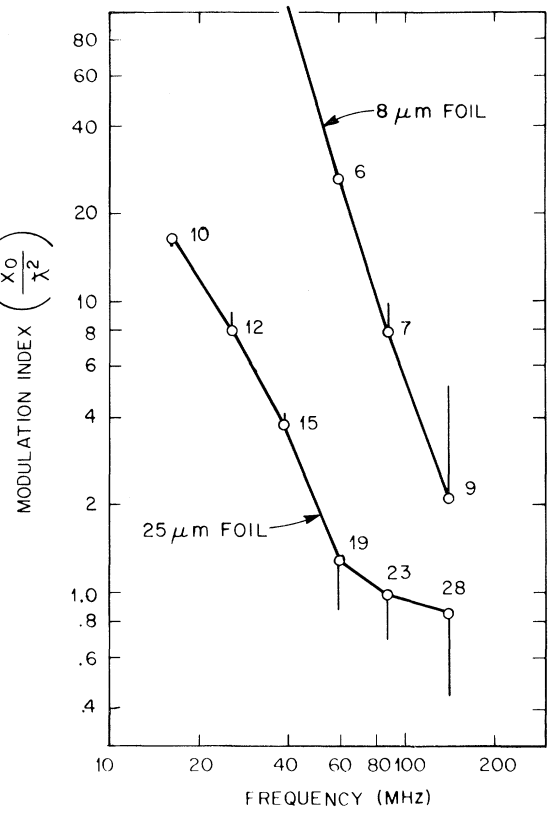

FIG. 11. Experimentally derived sideband modulation index parameters plotted as a function of driving frequency. The modulation indices plotted here are derived from the data of Figs. 2 and 3 by the procedure discussed in the text.

varies substantially over the range of frequency shown in Fig. 11 so that the 25-μm iron foil which is 20 skin depths thick at 16 MHz becomes 56 skin depths thick at 138 MHz. For reference, the calculated number of rf skin depths *to the center of the foil* is printed near each modulation index in Fig. 11. The significance of these numbers will be discussed in the next section.

MAGNETOSTRICTION MODEL

The experimental evidence just discussed narrowly limits the choice of possible formation mechanisms for rf sidebands. Ruled out are those models which do not attribute the sidebands to acoustic vibrations (e.g., Mitin's recent double-photon-resonance model[23]) or those models which invoke the motion of ferromagnetic domain walls (e.g., the domain-wall passage model already discussed). The experiments strongly indicate that sidebands result from the generation of internal acoustic vibrations which in turn are due to the rotation of the magnetization vector by the rf magnetic field. A model which is consistent with these facts is the model of magnetostriction.

The interaction between neighboring atomic magnetic moments which gives rise to magnetostriction has the form

$$f(r)\,(\cos^2\varphi - \tfrac{1}{3})\,,$$

depending on both the separation r and on the angle that the aligned moments make with respect to $\vec{r}$.[24] Thus the interaction tends to distort the crystal lattice. The distortion of the lattice proceeds until an equilibrium is reached with the opposing elastic restoring forces of the strained lattice.

It is characteristic of magnetostriction, because of the $\cos^2\varphi$ dependence of the interaction, that large changes in lattice shape occur during *rotations* of the domain magnetization, but that movement of 180° domain walls has little magnetostrictive effect. On this basis one can see why the large $\vec{H}_0$ field perpendicular to the perturbing field $\vec{H}_{rf}$ of Fig. 9 has only a small effect on sideband formation. When $\vec{H}_0$ and $\vec{H}_{rf}$ are perpendicular, their vector sum is a time-varying rotating field oscillating about $\vec{H}_0$ in the plane of the sample foil. This large rotating applied field causes the sample magnetization to rotate even more easily than it would if $\vec{H}_0$ were zero, thus accounting for the slightly larger sideband effect observed with $\vec{H}_0$ fields of 80 and 320 Oe. When the $\vec{H}_0$ field is increased to 1000 Oe, however, the angle through which the resultant vector sum oscillates becomes smaller. This reduces the magnetostrictive distortion and therefore according to the model also the sideband effect.

If, on the other hand, $\vec{H}_0$ is aligned parallel to $\vec{H}_{rf}$, then the possibilities for rotation of the domain magnetization become substantially reduced as the sample approaches magnetic saturation along $\vec{H}_0$. This, of course, is just the reason that the static magnetostrictive strain for any material approaches a limiting saturation value for large applied fields.[25] Thus the magnetostrictive model predicts that the sideband effect will decrease rapidly with increasing $\vec{H}_0$ provided $\vec{H}_0$ and $\vec{H}_{rf}$ are parallel. This is just what happens experimentally as was shown in Fig. 10.

In view of the rather good qualitative agreement on this point, it is appropriate to ask whether magnetostriction can satisfactorily account for other more quantitative characteristics of the sideband effect. A truly rigorous calculation is clearly out of the question, since it would require knowledge of the radio-frequency magnetoelastic-coupling tensor and the vibrational dynamics of the samples as mechanically mounted for these experiments. Therefore, we propose a formulation based on the following simplifying assumptions: (i) The magnetostrictive strain $\epsilon = \delta l/l$ is describable by a static isotropic model[24]

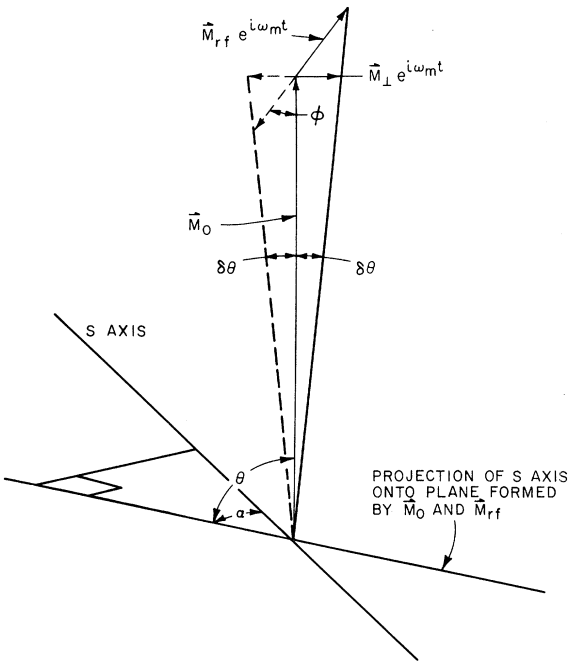

FIG. 12. Geometry relating the time-varying rf field to the axis s, along which the magnetostrictive strain is measured.

$$\delta l/l = \tfrac{3}{2}\,\Lambda\cos^2\theta\ , \tag{3}$$

where Λ is the saturated magnetostrictive constant of the material and θ is the angle between the magnetization vector and the direction in which the strain is measured; (ii) the radio-frequency component of the magnetization $\vec{M}_{rf}e^{i\omega_m t}$ is much smaller than the static magnetization $\vec{M}_0$; (iii) the measured static magnetostrictive constants are appropriate at radio frequencies; and (iv) any acoustic vibrations generated by the rf propagate in the material interacting with grain boundaries, surfaces, and crystal dislocations, the result of this being that the vibrations develop components along directions other than their initial direction.

Under these assumptions, $\vec{M}_{rf}\,e^{i\omega_m t}$ produces a small time variation $\delta\theta$ in the angle θ. Referring to Fig. 12 for the definition of $\vec{M}_\perp$ which is the component of $\vec{M}_{rf}$ that is perpendicular to $\vec{M}_0$, it is readily verified that

$$\delta\theta(t) \approx \frac{|\vec{M}_\perp|}{|\vec{M}_0|}\, e^{i\omega_m t} \approx \frac{|\vec{M}_0\times\vec{M}_{rf}|}{|\vec{M}_0|^2}\, e^{i\omega_m t}\ . \tag{4}$$

In the general case where the measurement axis s is at an angle α with respect to the plane formed by $\vec{M}_{rf}$ and $\vec{M}_0$, this expression becomes

$$\delta\theta(t) \approx \frac{|\vec{M}_0\times\vec{M}_{rf}|}{|\vec{M}_0|^2}\,(\cos\alpha)\, e^{i\omega_m t}\ . \tag{5}$$

The vector $\vec{M}_0$ here refers to the local saturation magnetization and may point in different directions in different parts of the sample.

The magnetostrictive strain is then

$$\epsilon(t) = \tfrac{3}{2}\,\Lambda\cos^2[\theta - \delta\theta(t)]\ , \tag{6}$$

or by trigonometric identity

$$\epsilon(t) = \tfrac{3}{2}\,\Lambda[\cos\theta\cos\delta\theta(t) + \sin\theta\sin\delta\theta(t)]^2\ . \tag{7}$$

Now using the small-angle trigonometric approximations, saving terms to order $[\delta\theta(t)]^2$, we obtain for the time-dependent part of the magnetostrictive strain

$$\frac{\delta l(t)}{l} \approx \tfrac{3}{2}\,\Lambda\left(\frac{|\vec{M}_0\times\vec{M}_{rf}|}{|\vec{M}_0|^2}\, e^{i\omega_m t}\sin 2\theta\cos\alpha - \frac{|\vec{M}_0\times\vec{M}_{rf}|^2}{|\vec{M}_0|^4}\, e^{i2\omega_m t}\cos 2\theta\cos^2\alpha\right)\ . \tag{8}$$

This expression for the rf magnetostrictive strain shows explicitly that sidebands are generated only by the component of $\vec{M}_{rf}$ that is perpendicular to $\vec{M}_0$. As pointed out earlier, this is in complete agreement with the magnetic field dependence observed experimentally.

The expression also indicates that magnetostrictive oscillations will be generated at the frequency $2\omega_m$ as well as at the driving frequency ω_m. But it should be remembered that assumption (ii) is generally valid for these experiments so that $|\vec{M}_{rf}| \ll |\vec{M}_0|$. Therefore, the harmonic term in Eq. (8) will nearly always be negligible in comparison with the first term.

The third property of Eq. (8) is the directionality of the rf strain implied by the trigonometric factors in θ and α. Unless the sample is magnetically saturated, however, the direction of $\vec{M}_0$ is distributed more or less at random in the sample so that averages over θ and α should be taken. An averaging over angles is also implied to the extent that assumption (iv) is valid. If the scattering of the rf acoustic waves changes the direction of the initial vibrational amplitudes, then even for a magnetically saturated single crystal, one would expect the angular effects to be partially washed out. Finally it should be recalled that expression (8) was obtained using a simplified isotropic model for the magnetostrictive strain. In the general anisotropic case the angular effects would undoubtedly be modified.

Let us now relate the magnetostriction model to the earlier sideband formalism by noting that $\delta l(t)$ corresponds approximately to the Doppler amplitude $x(t)$. Thus the calculation of the modulation index m of Eq. (1) or m^2 of Eq. (2) becomes

$$m^2 = \frac{x_0^2}{\lambda^2} \approx \frac{1}{\lambda^2}\left(\tfrac{3}{2}\,l\Lambda\,\frac{|\vec{M}_0\times\vec{M}_{rf}|}{|\vec{M}_0|^2}\right)^2\ . \tag{9}$$

To obtain an order-of-magnitude estimate of the index m, we note that $|\tilde{M}_{rf}| \approx \mu_{rot} |\tilde{H}_{rf}|$, where μ_{rot} is the initial permeability of the sample due only to rotation of the magnetization.[26] For iron metal[26] $\mu_{rot} \approx 29$ G/Oe, $|\tilde{M}_0| = 21.5$ kG, and $\Lambda = 20 \times 10^{-6}$. For the experimental conditions of the data in Fig. 2 we have $H_{rf} = 7.5$ Oe, with a disk-shaped iron-foil absorber 25 μm thick by 1.3 cm in diameter.

The remaining unspecified parameter is l, the sample dimension before the rf is applied. To form Mössbauer sidebands, the rf Doppler motion of the absorber nuclei must be *along* the γ-ray axis—that is, transverse to the plane of the absorber foil. For this reason one might assume that the proper choice for l is one-half the foil thickness. In this case only magnetostrictive changes in the foil thickness would be important, because presumably it is only this motion that is along the γ-ray axis. Substituting this 12.5-μm half-thickness together with the other numerical values into Eq. (9), however, results in a very small Doppler amplitude of 0.04 Å corresponding to a modulation index $m^2 \leq 0.08$. The experimental modulation indices for the data of Fig. 2, however, range between 0.5 and 18 (see Fig. 11). Thus the calculation produces a result which is at least an order of magnitude too small. The discrepancy becomes even more apparent for the thinner foil of Fig. 3.

Other authors[13,14] have found similar difficulties, and for this reason they abandoned[13] the model of magnetostriction.

However, if assumption (iv) listed above is valid, it is not at all necessary to abandon the magnetostrictive model. One can then assume following Eq. (8) that the initial rf magnetostrictive strain is large and primarily *in the plane* of the sample foil. Then invoking assumption (iv), one would expect after the acoustic waves propagate and scatter within the foil that some vibrational amplitudes will come to have components along the γ-ray axis. The sample foil can be pictured as a polycrystalline drumhead which if stretched and contracted along some diameter will also acquire vibrational modes along both axes normal to the original excitation.

The l dependence of Eq. (9) leads naturally to magnetostrictive displacements that are large in the plane of the foil, since in this plane l is also effectively large. If the entire 1.3-cm-diam sample referred to above were to respond magnetostrictively to the rf with the proper phase, for example, vibrational amplitudes of up to 20 Å would be generated producing enormous effective modulation indices transverse to the γ rays. Thus the problem is not that the magnetostrictive Doppler motion is small, but rather that the motion is not induced along the required axis. As stated above, assumption (iv) overcomes this difficulty.

Because the magnetostrictive amplitudes induced in the sample plane are so large, the postulated scattering processes need not be efficient. Even a weak oblique scattering effect which converted only a few percent of the planar rf strain to the transverse direction would be sufficient. We will now review the experimental evidence that indicates the acoustic-scattering mechanism that we postulate is reasonable.

We will discuss first the experimental evidence for the assertion that the rf acoustic waves propagate from one region to another within the sample. This evidence is provided by the sideband-frequency data for the metallic iron foils of Figs. 2 and 3 as summarized in Fig. 11. As mentioned in the last section, the numbers printed near each of the experimental modulation indices in Fig. 11 refer to the number of calculated rf skin depths from the surface to the center of the sample foil.

In looking at these numbers, it is well to remember that in a distance of only two skin depths the rf field is reduced to 13% of its original value. One would therefore expect the domain magnetization to rotate following the applied rf only in the extreme surface regions of the iron foil. It would appear from this that all of the significant magnetostrictive motion also occurs only in the thin-skin-depth region near the foil surface.

But the Mössbauer technique is sensitive to all of the Fe^{57} nuclei throughout the sample volume, not just those in the surface regions where the rf magnetostrictive vibrations presumably originate. Further, from the size of the rf-sideband effect observed, it is clear that a substantial fraction of *all* of the sample nuclei is vibrating at the applied frequency.

This is direct experimental support for the propagation of acoustic waves, because propagation of the acoustic vibrations is clearly required if all of the significant magnetostriction occurs in the skin-depth region, and yet the Doppler vibrations are felt throughout the sample volume.

The interpretation of the rf skin depth is somewhat complicated, however, by the possibility that spin waves might be generated in the iron foil by the rf field. If spin waves are generated in these experiments, they can carry the time-varying magnetization induced by the rf field into the metal sample beyond the rf skin depth. The rf skin depth would in effect be replaced by the presumably larger propagation depth for the spin waves. Deeper effective rf penetration by spin-wave propagation would, of course, improve the magnetostrictive coupling to the sample, but at the same time it would make the arguments for acoustic propagation somewhat less secure. Supplementary experiments were done which should have been sensitive to possible spin-wave-resonance effects

in sideband experiments. No evidence for spin waves was found.

Other experimental results also lend support to the acoustic-scattering hypothesis and the sideband model that we have developed using it. The model requires that rf magnetostrictive oscillations with displacements in the sample plane be large compared to those with displacements normal to it. The proposed propagation and scattering of the resulting acoustic vibrations will tend to equalize these tangential and normal oscillation amplitudes, but presumably with an efficiency of considerably less than one. The experimental data of Fig. 5 showing the sideband effect as a function of the angle between plane of the absorber and the axis of the γ rays confirm these expectations. In these data the sideband effect is seen to increase as predicted when the absorber plane is tilted toward the γ rays.

We shall now discuss briefly the other assumptions used in our model. The assumption of isotropic magnetostriction in our sample is a simplifying assumption which we have found convenient; however, it is not essential to the model. Assumption (ii) is undoubtedly valid for the experiments reported here. In iron, for example, the induced rf magnetization is of the order of 250 G, which is to be compared to the locally saturated domain magnetization of 21 500 G. Assumption (iii) is also not essential for the model. It is, however, supported by data in Bozorth, [27] which show that the magnetostrictive strain from an oscillating field approaches at high inductions the slope of the static $\Delta l/l$-vs-H magnetostriction curve.

Before completing the discussion of the magnetostriction model, we shall comment briefly on the acoustic internal friction of our samples. The internal friction Q^{-1} is a measure of the acoustic damping in a material. In measurements of Q^{-1} the sample is driven with a burst of acoustic waves. Numerically Q, the reciprocal of the internal friction, is the number of cycles which occur after the driving excitation is removed and before the acoustic amplitude is reduced to e^{-1} of its initial value.

It is found experimentally that Q is a strong function of the sample material, of the way the sample is mounted, and of the exciting frequency. For freely supported metal samples, Q is of the order of 10^2 or 10^3, whereas for materials similar to hematite values as high as 10^6 have been measured. However, these values are not applicable to the Mössbauer absorbers in our sideband experiments, because in an absorber the sample material is of necessity severely damped by its mounting. Nevertheless, it is certainly possible that the acoustic Q of our absorbers is greater than unity. In the discussion of the magnetostriction model just given, the absorbers were tacitly assumed to have an acoustic Q of one. If the Q values are larger, the required rf driving strain from magnetostriction would be reduced; the magnetostriction model would then enjoy a still larger numerical cushion.

DISCUSSION AND SUMMARY

The magnetostriction model of the last section provides a reasonably complete physical description of the phenomenon of rf Mössbauer sidebands. The model appears to account not only for all of the experiments of this paper, but also for the experiments of Perlow and of Matthias that were described in the Introduction. Concluding the discussion that was begun there, recall that Perlow[13] observed a general washing out of the Mössbauer absorption pattern when either Permalloy or Supermalloy foils were subjected to rf fields at 4.2 or 6.5 MHz. His results one might note are not unlike the spectra in our Fig. 4. Although he was able to fit his data to FM theory, he felt his results were more likely attributable to random flipping of the hyperfine field. We initiated a series of experiments with Permalloy in the hope of resolving the ambiguity on the interpretation. We were able to reproduce Perlow's results with rf fields at 4.2 MHz, and also with fields at 6.5 MHz. When we raised the frequency still further, however, we observed clearly resolved FM sidebands. For this reason we believe the effects reported by Perlow are due to magnetostrictive sidebands.

We are also confident that the rf-sideband effect provides a consistent explanation of the resonance effects reported by Matthias.[10] In the Matthias experiment, which was also described in the Introduction, the formation of rf sidebands in the iron source spreads the recoillessly emitted γ rays among many more lines. This reduces the effectiveness of the Mössbauer absorber, thus accounting for the increase in the nonresonant count rate when the rf is switched on. At the resonance frequencies of 26.0 or 45.5 MHz, however, the emission sidebands overlap some of the neighboring normal hyperfine lines so that there is a partial restoration of the Mössbauer absorption. We believe that this restoration due to sideband overlap was responsible for the resonance effects reported by Matthias.

This resonance experiment illustrates the subtle way in which sideband effects may be mistaken for nuclear magnetic resonance (NMR) effects. As it developed, NMR transitions at 26.0 MHz later were observed in the 100-nsec Mössbauer level of Fe^{57}. The observation of NMR-Mössbauer double resonance[28] became possible only after the competing sideband-overlap effects were suppressed by using finely powdered iron samples.

In summary, the following points have been established: Application of rf magnetic fields to ferro-

magnetic samples produces FM sidebands in the Mössbauer spectra of those samples. The sidebands are due to acoustic vibrations originating from within the sample and can be made to vanish by making the sample dimensions much smaller than the acoustic wavelength. A mechanism has been proposed which physically describes how the acoustic vibrations are generated in the sample by the applied rf magnetic field. The proposed model is based on rf magnetostriction. It is a simple first-order theory, but it appears to account qualitatively for all of the experimental observations.

ACKNOWLEDGMENTS

The authors would like to thank Charles P. Lichtenwalner and Vincent Turco of Bell Laboratories and Richard Guarnieri and Russell MacCauley of Johns Hopkins for technical help. One of the authors (L. N. P.) would also like to thank Dr. V. Jaccarino and Dr. J. F. Dillon, Jr. for helpful discussions.

APPENDIX

The quantum-mechanical formalism of FM sidebands in Mössbauer spectra can be made completely general, and the equivalence of the classical and quantum-mechanical descriptions can be clearly established in a straightforward manner by starting with a form of the Lamb-Mössbauer transition probability[29] that does not specify the type of averaging process to be employed, i.e.,

$$W(E) \propto \sum_a g(a) \sum_b \prod_{s=1}^{3N} \frac{|\langle b_s | e^{i\vec{p}\cdot\vec{x}/\hbar} | a_s \rangle|^2}{[E - E_0 - \sum_s (b_s - a_s)\hbar\omega_s]^2 + \frac{1}{4}\Gamma^2} \quad . \tag{A1}$$

This is simply Eq. (11) from Lamb's original neutron-capture paper[29] rewritten in the somewhat more transparent notation of Visscher.[30] To explicitly show the rf phonon mode ω_m, we can rewrite this expression as follows:

$$W'(E) \propto \sum_a g(a) \sum_b \sum_{a_m} \sum_{b_m} \prod_{s=1}^{3N} g(a_m) |\langle b_m | e^{i\vec{p}\cdot\vec{x}/\hbar} | a_m \rangle|^2 \frac{|\langle b_s | e^{i\vec{p}\cdot\vec{x}/\hbar} | a_s \rangle|^2}{[E_0 - E - \sum_s (b_s - a_s)\hbar\omega_s - (b_m - a_m)\hbar\omega_m]^2 + \frac{1}{4}\Gamma^2} \quad , \tag{A2}$$

where the additional sums are over the occupation numbers of the rf ultrasonic mode ω_m. By defining

$$n = b_m - a_m \ ,$$

Eq. (A2) can be transformed to

$$W'(E) = \sum_{n=-\infty}^{\infty} W(E - n\hbar\omega_m) \times \sum_{a_m} g(a_m) |\langle a_m + n | e^{i\vec{p}\cdot\vec{x}/\hbar} | a_m \rangle|^2 \ . \tag{A3}$$

The matrix element for each n can be evaluated by writing $\vec{x}$ in terms of annihilation and creation operators:

$$|\langle a_m + n | e^{ip\cos\varphi(\alpha+\alpha^\dagger)/(2MN\hbar\omega_m)^{1/2}} | a_m \rangle|^2 \ .$$

For example, consider $n = 0$ and expand the exponential in a power series. Since the initial and final states are the same, only even-power terms are nonzero:

$$\left|1 - \frac{1}{2!}\left(\frac{(p\cos\varphi)^2}{2MN\hbar\omega_m}\right)\langle a_m | (\alpha + \alpha^\dagger)^2 | a_m \rangle + \frac{1}{4!}\left(\frac{(p\cos\varphi)^2}{2MN\hbar\omega_m}\right)^2 \langle a_m | (\alpha + \alpha^\dagger)^4 | a_m \rangle + \cdots \right|^2 .$$

Now

$$\langle a_m | (\alpha + \alpha^\dagger)^2 | a_m \rangle = 2a_m + 1 \ . \tag{A4}$$

Similarly,

$$\langle a_m | (\alpha + \alpha^\dagger)^4 | a_m \rangle = 6a_m^2 + 6a_m - 3 \ . \tag{A5}$$

Higher-order terms may be calculated in a like manner. Also a_m and N are much greater than 1; consequently, only the highest power of a_m need be retained in each term. Since $p^2 = \hbar^2/\lambda^2$ the series can now be written

$$\left|1 - \left(\frac{\hbar a_m \cos^2\varphi}{2MN\omega_m\lambda^2}\right) + \frac{1}{4}\left(\frac{\hbar a_m \cos^2\varphi}{2MN\omega_m\lambda^2}\right)^2 - \frac{1}{36}\left(\frac{\hbar a_m \cos^2\varphi}{2MN\omega_m\lambda^2}\right) + \cdots \right|$$

$$= 1 - 2\left(\frac{\hbar a_m \cos^2\varphi}{2MN\omega_m\lambda^2}\right) + \frac{3}{2}\left(\frac{\hbar a_m \cos^2\varphi}{2MN\omega_m\lambda^2}\right)^2 - \frac{5}{6}\left(\frac{\hbar a_m \cos^2\varphi}{2MN\omega_m\lambda^2}\right) + \cdots$$

$$= J_0^2\{(2\hbar a_m \cos^2\varphi/MN\omega_m\lambda^2)^{1/2}\} .$$

Results for other values of n can be obtained in a similar manner and yield

$$J_n^2((2\hbar a_m \cos^2\varphi/MN\omega_m\lambda^2)^{1/2}) \ .$$

Consequently, we have

$$W'(E)=\sum_{n=-\infty}^{\infty} W(E-n\hbar\omega_m) \times \sum_{a_m} g(a_m) J_n^2((2\hbar a_m \cos^2\varphi/MN\omega_m \lambda^2)^{1/2}) . \tag{A6}$$

Because of the condition that $a_m \gg 1$, the sum over a_m can be replaced by an integral. Furthermore, for a harmonic oscillator, the amplitude of vibration in the direction of the radiation is $x_0=(2\bar{x}^2)^{1/2} = (2\hbar a_m \cos^2\varphi/MN\omega_m)^{1/2}$. With this correspondence Eq. (A3) becomes

$$W'(E)=\sum_{n=-\infty}^{\infty} W(E-n\hbar\omega_m)\int_0^{\infty} P(x_0) J_n^2\left(\frac{x_0}{\lambda}\right) dx_0 , \tag{A7}$$

which is Eq. (1) of the text.

The classical and quantum-mechanical formalisms are thus seen to be entirely equivalent, and in addition it is seen that the only factor that determines the functional description of the sideband intensities is the distribution of amplitudes (or equivalently the distribution of the ultrasonic phonon quantum numbers). For physically realizable situations, the distribution of amplitudes can be a Dirac δ function which gives $J_n^2(x_0/\lambda)$, a Rayleigh distribution which gives $e^{x_0^2/2\lambda^2} I_n(x_0^2/2\lambda^2)$, or one of an infinity of other possible functions.

---

*Portion of this work done at The College of William and Mary was supported by a National Science Foundation Departmental Development Grant.

†Portion done at the Johns Hopkins University was supported by a grant from the Atomic Energy Commission.

[1]N. Heiman, L. Pfeiffer, and J. C. Walker, Phys. Rev. Letters 21, 93 (1968).

[2]N. Heiman, L. Pfeiffer, and J. C. Walker, J. Appl. Phys. 40, 1410 (1969).

[3]N. Heiman, L. Pfeiffer, and J. C. Walker, in *Mössbauer Effect Methodology*, edited by I. Gruverman (Plenum, New York, 1971), Vol. VI.

[4]S. Goldman, *Frequency Analysis, Modulation and Noise* (McGraw-Hill, New York, 1948).

[5]S. L. Ruby and D. I. Bolef, Phys. Rev. Letters 5, 5 (1960).

[6]V. Burov, V. Krasilnikov, and O. Sukharevskaya, Zh. Eksperim. i Teor. Fiz. 43, 1184 (1962) [Sov. Phys. JETP 16, 837 (1963)].

[7]T. E. Cranshaw and P. Reivari, Proc. Phys. Soc. (London) 90, 1059 (1967).

[8]L. Mishory and D. Bolef, in *Mössbauer Effect Methodology*, edited by I. Gruverman (Plenum, New York, 1968), Vol. IV.

[9]G. Perlow, University of Illinois Report No. AFOSR TN 0-98, 1960 (unpublished).

[10]E. Matthias, in *Hyperfine Interactions and Nuclear Radiations*, edited by E. Matthias and D. Shirley (North-Holland, Amsterdam, 1968).

[11]M. Hack and M. Hammermesh, Nuovo Cimento 19, 54 (1961).

[12]H. Gabriel, Phys. Rev. 184, 359 (1969).

[13]G. Perlow, Phys. Rev. 172, 319 (1968).

[14]G. Asti, G. Albanese, and C. Bucci, Phys. Rev. 184, 260 (1969).

[15]L. Pfeiffer, in *Mössbauer Effect Methodology*, edited by I. Gruverman (Plenum, New York, 1972), Vol. VII.

[16]A. Abragam, *L'Effet Mössbauer* (Gordon and Breach, New York, 1964), pp. 22–24.

[17]A. Gossard, A. Portis, and W. Sandle, J. Phys. Chem. Solids 17, 341 (1961).

[18]L. Pfeiffer, in *Proceedings of the Seventeenth Conference on Magnetism and Magnetic Materials, Chicago*, 1971 (AIP, New York, 1972).

[19]M. Gaerttner, W. Wallace, and B. Maxfield, Phys. Rev. 184, 702 (1969).

[20]E. Dobbs, J. Phys. Chem. Solids 31, 1657 (1970).

[21]M. Gaerttner and B. Maxfield, Phys. Rev. Letters 26, 119 (1971).

[22]M. Eibschütz, L. Pfeiffer, and J. W. Nielson, J. Appl. Phys. 41, 1276 (1970).

[23]V. Mitin, Dokl. Akad. Nauk SSSR 194, 59 (1970) [Sov. Phys. Doklady 15, 827 (1971)].

[24]S. Chikazumi, *Physics of Magnetism* (Wiley, New York, 1964), Chap. 8.

[25]R. M. Bozorth, *Ferromagnetism* (Van Nostrand, Princeton, N. J., 1951), Chap. 13.

[26]S. Chikazumi, in Ref. 24, p. 263.

[27]R. M. Bozorth, in Ref. 25, pp. 639–641.

[28]N. Heiman, J. Walker, and L. Pfeiffer, Phys. Rev. 184, 281 (1969).

[29]W. E. Lamb, Phys. Rev. 55, 190 (1939).

[30]W. M. Visscher, Ann. Phys. (N. Y.) 9, 194 (1960).

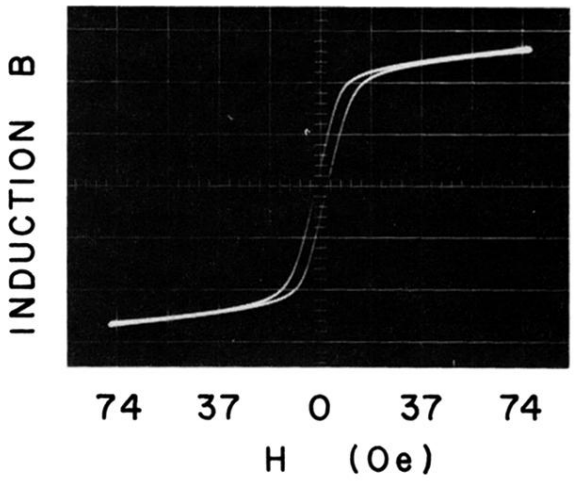

FIG. 8. $\vec{B}-\vec{H}$ hysteresis loop of the 8-μ-thick annealed iron foil used for the static-field experiments of Figs. 9 and 10. The loop shown was traced at a 60-Hz repetition rate.